LETTER

Wigner molecules and hybrid qubits

To cite this article: Constantine Yannouleas and Uzi Landman 2022 *J. Phys.: Condens. Matter* **34** 21LT01

Letters

IOP Publishing

Journal of Physics: Condensed Matter

J. Phys.: Condens. Matter **34** (2022) 21LT01 (6pp)

https://doi.org/10.1088/1361-648X/ac5c28

Letter

Wigner molecules and hybrid qubits

Constantine Yannouleas* **and Uzi Landman**

School of Physics, Georgia Institute of Technology, Atlanta, Georgia 30332-0430

E-mail: Constantine.Yannouleas@physics.gatech.edu and Uzi.Landman@physics.gatech.edu

Received 28 December 2021, revised 5 March 2022
Accepted for publication 9 March 2022
Published 28 March 2022

Abstract

It is demonstrated that exact diagonalization of the microscopic many-body Hamiltonian via systematic full configuration-interaction (FCI) calculations is able to predict the spectra as a function of detuning of three-electron hybrid qubits based on GaAs asymmetric double quantum dots (QDs). It is further shown that, as a result of strong inter-electron correlations, these spectroscopic patterns, including avoided crossings between states associated with different electron occupancies of the left and right wells, are inextricably related to the formation of Wigner molecules (WMs). These physical entities cannot be captured by the previously employed independent-particle or Hubbard-type theoretical modeling of the hybrid qubit. We report remarkable agreement with recent experimental results. Moreover, the present FCI methodology for multi-well QDs can be straightforwardly extended to treat Si/SiGe hybrid qubits, where the central role of WMs was recently experimentally confirmed as well.

Keywords: Wigner molecule, quantum-computer qubit, configuration interaction, three-electron double quantum dot, hybrid qubit

(Some figures may appear in colour only in the online journal)

1. Introduction

Effective design and optimal control of the operational manipulations and interplay between the various degrees of freedom defining single qubit gates, as well as multi-qubit architectures, are imperatives for efforts targeting the successful fabrication and implementation of quantum computing devices. To this aim major world-wide experimental endeavors (see, e.g., references [1–6]) have been undertaken during the last decade. This resulted in unprecedented progress in the development and employment of techniques for control and manipulation of the spin and charge which serve to characterize two-dimensional (2D) semiconductor-based three-electron hybrid-double-quantum-dot (HDQD) qubits [7–12]. Nonetheless, several recent experimental scrutinies on Si/SiGe [13] and GaAs [14] HDQD qubit devices provided unambiguous evidence (see also references [15, 16]) for the need to account, in modeling the qubit physics and performance, for the heretofore overlooked, but unavoidable, formation of Wigner molecules (WMs) [17–26], resulting from strong inter-electron (e–e) interactions, and the consequent rearrangement of the spectra of the qubit device with respect to that associated with non-interacting electrons.

The formation of WMs is outside the scope of investigations anchored in the framework of independent-particle (single-particle) modeling [7, 12, 27, 28], invoked at the very early stage of studies on 2D quantum dots (QDs) [29]. Nor are more involved Hubbard-type models [7, 30–35] adequate for the description of the formation of WMs and their physical consequences. Instead, it has been demonstrated in earlier theoretical treatments [17, 19, 20, 22–25, 36, 37] that the formation of WMs requires the employment of more comprehensive approaches, such as the symmetry-breaking/symmetry-restoration [17, 19, 22, 25] approach

* Author to whom any correspondence should be addressed.

or the full configuration-interaction (FCI) method (referred to also as exact diagonalization [20, 24, 25, 36, 37]).[1]

Here, motivated by the recent advances [8–14] in the fabrication of charge-spin HDQD qubits, we investigate the many-body spectra and wave functions of three electrons in an asymmetric two-dimensional double-well external confinement, implemented by a two-center-oscillator (TCO) potential [17, 22, 37]. In particular, we demonstrate the defining role that WM formation (associated with strong e-e correlations) play in shaping the spectra (including the key feature of a pair of left-right electron-occupancy-dependent avoided crossings) of semiconductor qubits by presenting the first FCI calculations for the case of a hybrid [7–14, 27] three-electron double-dot GaAs qubit with parameters comparable to those in reference [14].

Earlier fabricated GaAs QDs [28, 29, 38] were characterized by harmonic confinements with frequencies $\hbar\omega_0 \geqslant 3$ meV (with $R_{\rm W} < 1.97$; see equation (4)), which correspond to a range of smaller QD sizes that did not favor the observation of the WMs at zero magnetic fields [38]. The much larger anisotropic GaAs double dot of reference [14], as well as the findings of reference [13] concerning Si/SiGe dots, where strong WM signatures were observed, herald the exploration of heretofore untapped potentialities in the fabrication and control of QD qubits, an objective that the present paper aims to facilitate from a theory perspective.

2. Results

Many-body Hamiltonian: we consider a many-body Hamiltonian for N confined electrons of the form

$$\mathcal{H}_{\rm MB}(\mathbf{r}_i, \mathbf{r}_j) = \sum_{i=1}^{N} H_{\rm TCO}(i) + \sum_{i=1}^{N}\sum_{j>i}^{N} \frac{e^2}{\kappa|\mathbf{r}_i - \mathbf{r}_j|}, \qquad (1)$$

where $\mathbf{r}_i$, $\mathbf{r}_j$ denote the vector positions of the i and j electron, and κ is the dielectric constant of the semiconductor material.

The single-particle $H_{\rm TCO}$ [17, 22, 37] with the unindexed coordinates x and y corresponding to the confined particles [i = 1, . . . , N in equation (1)], is given by:

$$H_{\rm TCO} = \frac{\mathbf{p}^2}{2m^*} + \frac{1}{2}m^*\omega_y^2 y^2 + \frac{1}{2}m^*\omega_{xk}^2 x_k'^2 + V_{\rm neck}(x_k') + h_k, \qquad (2)$$

where $x_k' = x - x_k$ with $k = 1$ for $x < 0$ (left well) and $k = 2$ for $x > 0$ (right well), and the h_k's control the relative depth of the two wells, with the detuning defined as $\varepsilon = h_1 - h_2$. y denotes the coordinate perpendicular to the interdot axis (x). The most general shapes described by $H_{\rm TCO}$ are two semiellipses connected by a smooth neck [$V_{\rm neck}(x_k')$]. $x_1 < 0$ and $x_2 > 0$ are the centers of these semiellipses, $d = x_2 - x_1$ is the interdot distance, and m^* is the effective electron mass.

For the smooth neck, we use

$$V_{\rm neck}(x_k') = \frac{1}{2}m^*\omega_{xk}^2\left[\mathcal{C}_k x_k'^3 + \mathcal{D}_k x_k'^4\right]\theta(|x| - |x_k|), \qquad (3)$$

where $\theta(u) = 0$ for $u > 0$ and $\theta(u) = 1$ for $u < 0$. The four constants $\mathcal{C}_k$ and $\mathcal{D}_k$ can be expressed via two parameters, as follows: $\mathcal{C}_k = (2 - 4\epsilon_k^b)/x_k$, and $\mathcal{D}_k = (1 - 3\epsilon_k^b)/x_k^2$, where the barrier-control parameters $\epsilon_k^b = (V_b - h_k)/V_{0k}$ are related to the height of the targeted interdot barrier V_b (measured from the zero point of the energy scale), and $V_{0k} = m\omega_{xk}^2 x_k^2/2$. We note that measured from the bottom of the left ($k = 1$) or right ($k = 2$) well the interdot barrier is $V_b - h_k$.

$H_{\rm TCO}$ has the advantage of incorporating a smooth interdot barrier V_b, which can be varied independently of the interdot separation d; for an illustration see the inset of figure 1(a). Motivated by the asymmetric double-dot used in the GaAs device described in reference [14], we choose the parameters entering in the TCO Hamiltonian as follows: the left dot is elliptic with frequencies corresponding to $\hbar\omega_{x1} = 0.413\,567$ meV $= 100$ h · GHz (long x-axis) and $\hbar\omega_{y1} = \hbar\omega_y = 1.22$ meV $= 294.9945$ h · GHz (short y-axis), whereas the right dot is circular with $\hbar\omega_{x2} = \hbar\omega_{y2} = \hbar\omega_y = 1.22$ meV $= 294.9945$ h · GHz (1 h · GHz $= 4.135\,67$ μeV). The left dot is located at $x_1 = -120$ nm, and the right dot is located at $x_2 = 75$ nm. The detuning parameter is defined as $\varepsilon = h_1 - h_2$, where h_1 and h_2 are the chemical potentials of the left and right dot, respectively. The interdot barrier from the bottom of the right dot is set to $V_b - h_2 = 3.3123$ meV $= 800.91$ h · GHz. Finally, the effective electron mass and the dielectric constant for GaAs are $m^* = 0.067m_{\rm e}$ and $\kappa = 12.5$, respectively.

The Wigner parameter: at zero magnetic field and in the case of a single circular harmonic QD, the degree of electron localization and Wigner-molecule pattern formation can be associated with the socalled Wigner parameter [17, 25]

$$R_{\rm W} = Q/(\hbar\omega_0), \qquad (4)$$

where Q is the Coulomb interaction strength and $\hbar\omega_0$ is the energy quantum of the harmonic potential confinement (being proportional to the one-particle kinetic energy); $Q = e^2/(\kappa l_0)$, with $l_0 = (\hbar/(m^*\omega_0))^{1/2}$ the spatial extension of the lowest state's wave function in the harmonic (parabolic) confinement.

Naturally, strong experimental signatures for the formation of WMs are not expected for values $R_{\rm W} < 1$. In the double dot under consideration here, there are two different energy scales, $\hbar\omega_1 = 0.413\,567$ meV (associated with the long x dimension of the left QD) and $\hbar\omega_2 = 1.22$ meV (associated with the right circular QD). As a result, for GaAs (with $\kappa = 12.5$) one gets two different values for the Wigner parameter, namely $R_{\rm W,1} = 5.31$ and $R_{\rm W,2} = 3.09$. These values suggest that a stronger WM should form in the left QD compared to the right QD, as indeed was found by the FCI calculation (see below).

CI spectra as a function of detuning: we use the three-part notation $(n_{\rm L}, n_{\rm R};\ S)$ to denote the left-well electron occupation, the right-well electron occupation, and the total spin, respectively; $S = 1/2$ or $S = 3/2$ for three electrons.

In figure 1(a), the low-energy spectrum in the GaAs case ($\kappa = 12.5$) is displayed in the range of detunings 1.40 meV $\leqslant \varepsilon \leqslant$ 2.1 meV. The $(2, 1;\ S)$ states with two electrons in the *left* well, along the $(1, 2;\ S)$ states with two electrons in the right well, are prominent. States with three electrons in a given well,

[1] For a detailed discussion of these two methodologies in the context of QDs, see the review article in reference [25].

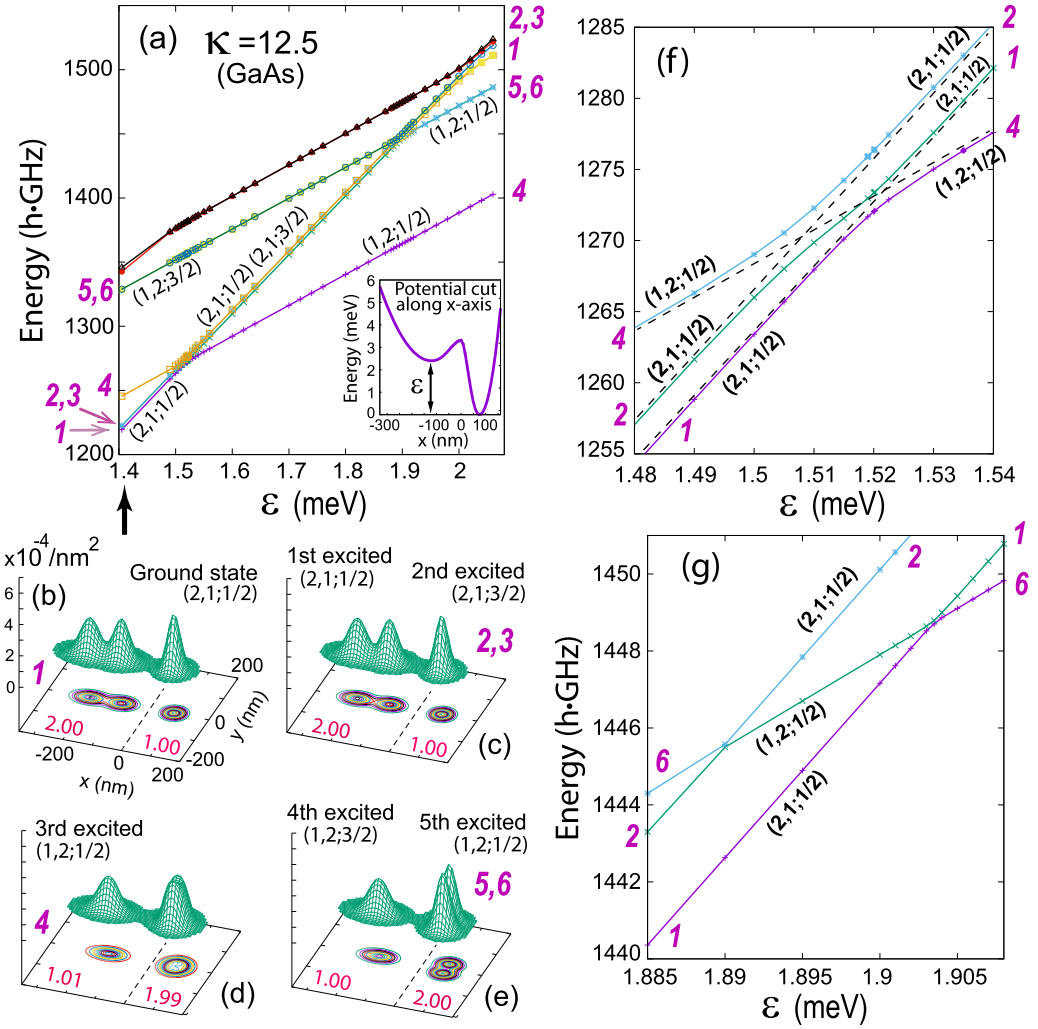

Figure 1. (a) Low-energy spectrum for the three-electron GaAs ($\kappa = 12.5$) double dot. The arrow indicates the value of the detuning at which the total charge densities were calculated. (b)–(e) Total charge densities for the ground and first five excited states. (f) and (g) Magnification of the neighborhoods of the CI avoided crossings appearing in (a). Only the $S = 1/2$ states, relevant to the hybrid qubit, are shown. The notation $(n_L, n_R;\ S)$ denotes the left electron occupation, the right electron occupation, and the total spin, respectively. For all densities, the scales of all three axes are as in (b). CI-calculated left and right occupations are highlighted in red.

associated with a notation $(3, 0;\ S)$ or $(0, 3;\ S)$, are absent. The fact that only the six $(2, 1;\ S)$ and $(1, 2;\ S)$ states comprise the lowest-energy spectrum for the GaAs double dot is an essential feature that is a prerequisite for the implementation of the hybrid qubit which uses [7, 8, 12, 14, 27] the four $(2, 1;\ 1/2)$ and $(2, 1;\ 1/2)$ states. As discussed below, this feature is brought about by the formation of WMs resulting from strengthening of the typical Coulomb interaction energies relative to the energy gaps in the single-particle spectrum of a confining external potential that represents a rather large-size and strongly asymmetric double dot (see the earlier discussion on the Wigner parameter R_W).

In figure 1(a), we have successively numbered the lowest six states at $\varepsilon = 1.4$ meV, starting from the ground state (#1) and moving upwards to the first five excited ones. Apart from the immediate neighborhood of an avoided crossing, these energy curves are straight lines, and naturally we extend the same numbering for all values of the detuning in the window range used in figure 1(a).

The spectrum in figure 1(a) requires additional commentary, because of quasi-degeneracies between the states #2, #3, and #5, #6, as well as the small energy gap ($\sim$3 h · GHz) between state #1 and the quasi-degenerate pair (#2, #3). We stress that the states #1 and #2 have two electrons in the *left* well and total spin $S = 1/2$, and thus they are denoted as $(2, 1;\ 1/2)$, whereas state #3 has two electrons in the left well, but a total spin of $S = 3/2$ (denoted as $(2, 1;\ 3/2)$). On the other hand, states #4, #6 (with $S = 1/2$), and #5 (with $S = 3/2$) have two electrons in the *right* well and they are denoted as $(1, 2;\ S)$. A main feature of this six-state spectrum in figure 1(a) is that, apart from the neighborhoods of the two avoided crossings, the energy curves for the states #1, #2, and #3 form one band of parallel lines, whereas the energy curves for the states #4, #5, and #6 form a second band of parallel lines, and the two bands intersect at two avoided crossings.

We reiterate that the appearance of such three-member bands, grouping together two $S = 1/2$ states and one $S = 3/2$

state, is a consequence of the formation of a 3e WM (three localized electrons considering both wells), and this organization is in consonance with the findings of reference [36] regarding the spectrum of three electrons in single anisotropic QDs in variable magnetic fields. We further stress that the dominant feature in the spectrum shown in figure 1(a) is the small energy gap between the two $S = 1/2$ states #1 and #2, which contrasts with the large gap between the other two $S = 1/2$ states #4 and #5, a behavior that agrees with the experimental findings of reference [14].

Charge densities away from the avoided crossings: further insights into the unique trends and properties of the GaAs HDQD qubit are gained through an inspection of the CI charge densities, plotted in figures 1(b)–(e) for the ground and first five excited states. The red numbers indicate the left-well and right-well electron occupations as calculated from the CI method. Naturally, the charge densities are normalized to the total number of electrons $N = 3$.

The charge densities deviate strongly from those expected from an independent-particle system. Indeed the formation of a strong 2e WM in the left well and of a weaker 2e WM in the right well is clearly seen through the emergence of a double hump in all six cases.

The avoided crossings: the position and the asymmetric anatomy of the two avoided crossings (figures 1(a), (f) and (g)) play an essential role in the operation of the hybrid qubit [14], requiring a FCI simulation that incorporates both dots of the HDQD qubit, as demonstrated here[2]. In figures 1(f) and (g), we display magnifications of the neighborhoods of the left and right CI avoided crossings, respectively, appearing in the spectrum of the GaAs double dot (figure 1(a)). Only the $S = 1/2$ states are shown, because the $S = 3/2$ states are not relevant for the workings of the hybrid qubit [7, 14, 35, 39].

The left avoided crossing (situated in the neighborhood of 1.49 meV $< \varepsilon <$ 1.54 meV) is formed through the interaction of the three curves #1, #2, and #4 (we keep the same numbering of the curves here as in figure 1(a)). On the other hand, the curves #1, #2, and #6 participate in the formation of the right avoided crossing in the neighborhood of 1.885 meV $< \varepsilon <$ 1.908 meV. We note that, according to the FCI calculation, the two avoided crossings are separated by a detuning distance of $\sim$400 μeV, which agrees with the experimentally determined value for the hybrid qubit device in reference [14].

The continuous lines in figures 1(f) and (g) represent the socalled *adiabatic* paths, which the system follows for slow time variations of the detuning. For fast time variations of the detuning, or with an applied laser pulse, the system can instead follow the *diabatic* paths indicated explicitly with dashed lines in figure 1(f) and thus jump from one adiabatic line to another; this occurs according to the celebrated Landau–Zener–Stückelberg–Majorana [40–42] dynamical interference theory.

[2] The qubit is initialized in the ground-state on line #4 (tuned to the far right of the left crossing) in figure 1(a). After detuning and laser-pulse-induced jumping to state #2 (at left crossing, figure 1(f)), readout is achieved via increased detuning, moving along state #1 and through the right avoided crossing to state #6 (figure 1(g)).

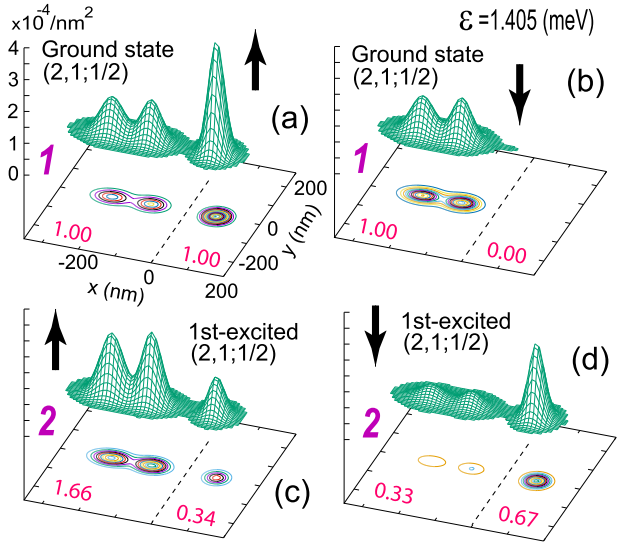

Figure 2. The spin structure of the ground state (a), (b) and 1st-excited (c) and (d) states at $\varepsilon = 1.405$ (see figures 1(b) and (c) for the corresponding total charge densities). The red numbers indicate the CI-calculated left and right occupancies (rounded to the second decimal point). The spin-resolved densities integrate to the number of spin-up and spin-down electrons in (a) and (b), respectively. The arrows indicate the spin direction.

Spin structure away from the avoided crossings: the charge densities associated with the states #1, #2, and #3 in the three-member band are designated with the same numbers and are plotted in the top two frames of figure 1(b). These three charge densities are very similar. However the corresponding spin structures are different. We analyze below the two cases of the ground state and the 1st-excited state for $\varepsilon = 1.405$ meV.

Figures 2(a) and (b) display the spin-up and spin-down densities for the ground state mentioned above; compare figure 1(b) for the total charge density. From these two spin-resolved densities, it is immediately seen that the spin structure of this ground state conforms to the following familiar expression [7, 14, 35, 36, 39] in the theory of three-electron qubits and QDs:

$$(|duu\rangle - |udu\rangle)/\sqrt{2}, \tag{5}$$

where u and d denote an up and down spin, respectively, with the three spins arranged from left to right in three ordered sites.

Figures 2(c) and (d) display the spin-up and spin-down densities for the associated 1st-excited state; compare figure 1(c) for the total charge density. From these two spin-resolved densities, one can conclude that the spin structure of this 1st-excited state conforms to a second familiar expression [7, 14, 35, 36, 39] in the theory of three-electron qubits and QDs, namely

$$(2|uud\rangle - |duu\rangle - |udu\rangle)/\sqrt{6}. \tag{6}$$

Indeed, from equation (6), one can derive that the expected spin-up occupancy for the most leftward and middle positions of the three spins is $5/6$ in both cases, yielding $5/3 =$

1.666 for the expected spin-up occupancy in the left dot, in agreement with the CI value of 1.66 highlighted in red in figure 2(c). Similarly the expected spin-up occupancy for the right dot from equation (6) is $1/3 = 0.333$, in agreement with the CI-value of 0.34 highlighted in red in figure 2(c). Moreover, from equation (6), one can derive that the expected spin-down occupancy for the most leftward and middle positions of the three spins is $1/6$ in both cases, yielding $1/3 = 0.333$ for the expected spin-down occupancy in the left dot, in agreement with the CI value of 0.33 highlighted in red in figure 2(d). Finally the expected spin-down occupancy for the right dot from equation (6) is $2/3 = 0.666$, in agreement with the CI-value of 0.67 highlighted in red in figure 2(d).

The effective matrix Hamiltonian: from the CI spectra, one can extract the phenomenological effective matrix Hamiltonian [8, 14] that has played a central role in the experimental dynamical control of the hybrid qubit. The general form of this 4×4 matrix Hamiltonian is:

$$H_M = \begin{pmatrix} c_L\widetilde{\varepsilon}/2 & 0 & \delta_1 & -\delta_2 \\ 0 & c_L\widetilde{\varepsilon}/2 + \Delta E_L & -\delta_3 & \delta_4 \\ \delta_1 & -\delta_3 & c_R\widetilde{\varepsilon}/2 & 0 \\ -\delta_2 & \delta_4 & 0 & c_R\widetilde{\varepsilon}/2 + \Delta E_R, \end{pmatrix} \tag{7}$$

where $\widetilde{\varepsilon} = \varepsilon - \varepsilon_0$ here denotes a renormalized detuning.

A good fit with the CI spectrum in figures 1(a), (f) and (g) is achieved by setting $c_L = 4.4$, $\Delta E_L = 15$ μeV, $c_R = 2.7$, $\Delta E_R = 340$ μeV, $\delta_1 = 0.657$ μeV, $\delta_2 = 0.090$ μeV, $\delta_3 = 1.207$ μeV, $\delta_4 = 0.075$ μeV, and $\varepsilon_0 = 1.50$ meV.

The effective matrix Hamiltonian in equation (7) reflects (within the plotted window) two properties of the FCI spectrum in figure 1(a) that are instrumental [8, 43] for the successful operation of the hybrid qubit, namely, the quasi-linear dependence of H_M on the detuning $\widetilde{\varepsilon}$ and the quasi-parallel behavior of both the two $(2, 1, 1/2)$ states (states #1 and #2) and the two $(1, 2, 1/2)$ states (states #4 and #6). We note a difference between references [8, 14] and the CI result for H_M, namely, references [8, 14] assume the values $c_L = 1$ and $c_R = -1$ associated with 45° and −45° slopes of the associated lines, respectively, while the CI result produces different slopes associated with $c_L = 4.4$ and $c_R = 2.7$.

3. Conclusions

We presented extensive FCI results that combine both energetics and investigation of the many-body wave functions through the calculation of charge and spin-resolved densities. Going beyond two-particle CI treatments in a single dot [13–16], this paper enabled for the first time the investigation of key features appearing in the low-energy spectrum of actual experimentally fabricated GaAs three-electron HDQD qubits, and in particular the role of a pair of avoided crossings between levels corresponding to different electron occupancies in the left and right wells. We demonstrated that the emergence of these spectral features, which are codified in a simple effective matrix Hamiltonian (equation (7)), emanating from the complexity of the many-body problem, is inextricably related to electron localization and the formation of WMs.

Derivations [7, 34] of the matrix Hamiltonian in equation (7), starting from approximate two-site Hubbard-type modeling, involve qualitative approximations which are not applicable for the case of WM formation. Consequently, the present CI-based confirmation of this effective matrix Hamiltonian, accounting fully for strong-correlation effects within each well and WM formation, is an unexpected auspicious result.

Our multi-dot FCI method can straightforwardly be expanded to incorporate the valley degree of freedom, thus holding the potential for being adopted as an effective tool for analysing and designing hybrid qubits, including the case of Si/SiGe hybrid qubits with more than three electrons where more complex spectra have been recently experimentally discovered [13]. In this context, a main focus of ongoing research [44] is the investigation of the effect of the valley degree of freedom on the formation of near-degenerate pairs of electronic states. We mention again that, in the case of the GaAs qubit device [14] considered here, the quasi-degeneracies is an effect of the strong e–e interaction and Wigner-molecule formation, which suppress the energy gaps in the electronic spectrum. The valley degree of freedom will introduce further possibilities for grouping of the electronic states of the qubit device due to additional group symmetries that become apparent when the valley-pseudospin analogy is explicitly considered; e.g., the $SU(4)$ or $SU(2) \times SU(2)$ group symmetries.

Acknowledgments

This work has been supported by a grant from the Air Force Office of Scientific Research (AFSOR) under Award No. FA9550-21-1-0198. Calculations were carried out at the GATECH Center for Computational Materials Science.

Data availability statement

All data that support the findings of this study are included within the article (and any supplementary files).

ORCID iDs

Constantine Yannouleas https://orcid.org/0000-0002-6320-3484
Uzi Landman https://orcid.org/0000-0002-1586-1554

References

[1] Hanson R, Kouwenhoven L P, Petta J R, Tarucha S and Vandersypen L M K 2007 *Rev. Mod. Phys.* **79** 1217
[2] Zwanenburg F A, Dzurak A S, Morello A, Simmons M Y, Hollenberg L C L, Klimeck G, Rogge S, Coppersmith S N and Eriksson M A 2013 *Rev. Mod. Phys.* **85** 961
[3] Barthel C, Kjærgård M, Medford J, Stopa M, Marcus C, Hanson M and Gossard A 2010 *Phys. Rev.* B **81** 161308(R)
[4] Morello A *et al* 2010 *Nature* **467** 687
[5] Orona L A, Nichol J M, Harvey S P, Bøttcher C G L, Fallahi S, Gardner G C, Manfra M J and Yacoby A 2018 *Phys. Rev.* B **98** 125404
[6] Medford J *et al* 2013 *Nat. Nanotechnol.* **8** 654

[7] Shi Z *et al* 2012 *Phys. Rev. Lett.* **108** 140503
[8] Shi Z *et al* 2014 *Nat. Commun.* **5** 3020
[9] Kim D, Ward D R, Simmons C B, Savage D E, Lagally M G, Friesen M, Coppersmith S N and Eriksson M A 2015 *npj Quantum Inf.* **1** 15004
[10] Cao G *et al* 2016 *Phys. Rev. Lett.* **116** 086801
[11] Thorgrimsson B *et al* 2017 *npj Quantum Inf.* **3** 32
[12] Chen B B, Wang B C, Cao G, Li H O, Xiao M, Guo G C, , Jiang H W, Hu X and Guo G P 2017 *Phys. Rev.* B **95** 035408
[13] Corrigan J *et al* 2021 *Phys. Rev. Lett.* **127** 127701
[14] Jang W *et al* 2021 *Nano Lett.* **21** 4999
[15] Ercan H E, Coppersmith S N and Friesen M 2021 *Phys. Rev.* B **104** 235302
[16] Abadillo-Uriel J C, Martinez B, Filippone M and Niquet Y-M 2021 *Phys. Rev.* B **104** 195305
[17] Yannouleas C and Landman U 1999 *Phys. Rev. Lett.* **82** 5325
[18] Egger R, Häusler W, Mak C H and Grabert H 1999 *Phys. Rev. Lett.* **82** 3320
[19] Yannouleas C and Landman U 2000 *Phys. Rev.* B **61** 15895
[20] Yannouleas C and Landman U 2000 *Phys. Rev. Lett.* **85** 1726
[21] Filinov A V, Bonitz M and Lozovik Y E 2001 *Phys. Rev. Lett.* **86** 3851
[22] Yannouleas C and Landman U 2002 *Int. J. Quantum Chem.* **90** 699
[23] Mikhailov S A 2002 *Phys. Rev.* B **65** 115312
[24] Ellenberger C, Ihn T, Yannouleas C, Landman U, Ensslin K, Driscoll D and Gossard A C 2006 *Phys. Rev. Lett.* **96** 126806
[25] Yannouleas C and Landman U 2007 *Rep. Prog. Phys.* **70** 2067
[26] Kalliakos S, Rontani M, Pellegrini V, García C P, Pinczuk A, Goldoni G, Molinari E, Pfeiffer L N and West K W 2008 *Nat. Phys.* **4** 467
[27] Kim D *et al* 2014 *Nature* **511** 70
[28] Bakker M A, Mehl S, Hiltunen T, Harju A and DiVincenzo D P 2015 *Phys. Rev.* B **91** 155425
[29] Kouwenhoven L P, Marcus C M, McEuen P L, Tarucha S, Westervelt R M and Wingreen N S 1997 Electron transport in quantum dots *Mesoscopic Electron Transport* (*Dordrecht: NATO ASI Series (Series E: Applied Sciences)* vol 345 ed L Sohn, L Kouwenhoven and G Schön (Berlin: Springer) pp 105–214
[30] Stafford C A and Das Sarma S 1994 *Phys. Rev. Lett.* **72** 3590
[31] Burkard G, Loss D and DiVincenzo D P 1999 *Phys. Rev.* B **59** 2070
[32] Yang S, Wang X and Sarma S D 2011 *Phys. Rev.* B **83** 161301(R)
[33] Das Sarma S, Wang X and Yang S 2011 *Phys. Rev.* B **83** 235314
[34] Ferraro E, De Michielis M, Mazzeo G, Fanciulli M and Prati E 2014 *Quantum Inf. Process.* **13** 1155
[35] Russ M and Burkard G 2017 *J. Phys.: Condens. Matter* **29** 393001
[36] Li Y, Yannouleas C and Landman U 2007 *Phys. Rev.* B **76** 245310
[37] Li Y, Yannouleas C and Landman U 2009 *Phys. Rev.* B **80** 045326
[38] Kouwenhoven L P, Austing D G and Tarucha S 2001 *Rep. Prog. Phys.* **64** 701
[39] DiVincenzo D P, Bacon D, Kempe J, Burkard G and Whaley K B 2000 *Nature* **408** 339
[40] Cao G, Li H-O, Tu T, Wang L, Zhou C, Xiao M, Guo G-C, Jiang H-W and Guo G-P 2013 *Nat. Commun.* **4** 1401
[41] Koh T S, Gamble J K, Friesen M, Eriksson M A and Coppersmith S N 2012 *Phys. Rev. Lett.* **109** 250503
[42] Ribeiro H, Petta J R and Burkard G 2013 *Phys. Rev.* B **87** 235318
[43] Wang B C, Cao G, Li H O, Xiao M, Guo G C, Hu X, Jiang H W and Guo G P 2017 *Phys. Rev. Appl.* **8** 064035
[44] Yannouleas C and Landman U unpublished